OPEN

Microbial Oxidation of Fe^{2+} and Pyrite Exposed to Flux of Micromolar H_2O_2 in Acidic Media

Yingqun Ma[1,3] & Chuxia Lin[2]

[1]Centre for Ecological and Environmental Technologies, South China Agricultural University, Guangzhou 510642 China, [2]Australian Centre for Sustainable Catchments, University of Southern Queensland, Toowoomba, QLD 4350 Australia, [3]National Key Laboratory of Environmental Criteria and Risk Assessment, Chinese Research Academy of Environmental Sciences, Beijing, 100012, China.

At an initial pH of 2, while abiotic oxidation of aqueous Fe^{2+} was enhanced by a flux of H_2O_2 at micromolar concentrations, bio-oxidation of aqueous Fe^{2+} could be impeded due to oxidative stress/damage in *Acidithiobacillus ferrooxidans* caused by Fenton reaction-derived hydroxyl radical, particularly when the molar ratio of Fe^{2+} to H_2O_2 was low. When pyrite cubes were intermittently exposed to fluxes of micromolar H_2O_2, the reduced Fe^{2+}-Fe^{3+} conversion rate in the solution (due to reduced microbial activity) weakened the Fe^{3+}-catalyzed oxidation of cubic pyrite and added to relative importance of H_2O_2-driven oxidation in the corrosion of mineral surfaces for the treatments with high H_2O_2 doses. This had effects on reducing the build-up of a passivating coating layer on the mineral surfaces. Cell attachment to the mineral surfaces was only observed at the later stage of the experiment after the solutions became less favorable for the growth of planktonic bacteria.

Pyrite (FeS_2) commonly occurs in the Earth's surface environments[1]. Great efforts have been made for the past decades to understand the mechanisms and kinetics of pyrite oxidation[2–14], which is the driving force leading to the widespread ecological degradation caused by the formation of acid mine drainage (AMD) and acid sulfate soils (ASS)[15–17]. The established model to describe pyrite oxidation consists of the following overall chemical equations:

$$FeS_2 + 3.5O_2 + H_2O \rightarrow Fe^{2+} + 2SO_4{}^{2-} + 2H^+ \qquad (1)$$

$$4Fe^{2+} + O_2 + 4H^+ \rightarrow 4Fe^{3+} + 2H_2O \qquad (2)$$

$$FeS_2 + 14Fe^{3+} + 8H_2O \rightarrow 15Fe^{2+} + 2SO_4{}^{2-} + 16H^+ \qquad (3)$$
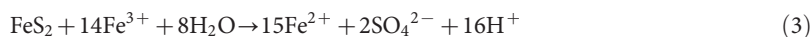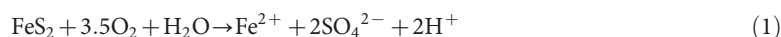
Initially, oxidation of pyrite by molecular oxygen results in generation of sulfuric acid and ferrous sulfate (Equation 1). This process only completes the conversion of pyrite-S from S^- to S^{6+}. The aqueous Fe^{2+} of pyrite origin may further react with molecular oxygen to form Fe^{3+} (Equation 2), which subsequently acts as a more effective oxidant for pyrite oxidation (Equation 3) if the pH is sufficiently low to prevent Fe^{3+} hydrolysis. Abiotic oxidation of Fe^{2+} is very slow under acidic conditions but the process can be catalyzed by iron-oxidizing bacteria[3].

Hydrogen peroxide (H_2O_2) is an aggressive oxidant and it is commonly present in rainwater[18–20], especially during thunderstorms[21]. H_2O_2 can also be generated through radiolysis of water in geological formations or industrial wastes containing radioactive materials such as uranium ores, spent nuclear fuel etc[22,23]. Therefore, contacts between H_2O_2 and pyrite grain surfaces or/and aqueous Fe^{2+} are likely to occur in natural environments. Moreover, H_2O_2 has potential applications in hydrometallurgy for the extraction of base metals from sulfide ores[24–26] and in desulfurization of coal[27]. There is therefore a possibility for the leaking/residual H_2O_2 to be in contact with pyrite in the non-target areas surrounding the heap leach piles. Furthermore, it was also suggested that H_2O_2 could be spontaneously generated when pyrite reacted with H_2O in the absence of oxygen[28] or during the oxidation of pyrite with molecular oxygen[29,30]. From a planetary perspective, the presence of atmospheric H_2O_2 in other planets such as Mars may represent an important factor that has been affecting the acid sulfate-producing processes in Martian environments[31].

It is well established that powerful oxidative intermediates (free radicals) are generated as a result of the chain reactions initiated by contact between H_2O_2 and Fe^{2+} i.e. so-called Fenton reactions[32,33]. Therefore, H_2O_2 may have a dual role to play: (a) as a strong oxidant for abiotic oxidation of pyrite and aqueous Fe^{2+}, and (b) as a toxicant (through the generation of free radicals) to cause oxidative stress in iron/sulfide-oxidizing bacteria and consequently affect their ability to catalyze Fe^{2+} oxidation.

Surface oxidation of pyrite by millimolar H_2O_2 (2–200 mmol L^{-1}) in molecular oxygen-free conditions has been examined by Lefticariu et al[34,35] in abiotic systems. The role of H_2O_2 spontaneously generated from oxidation of powdered pyrite by molecular oxygen was investigated by Schoonen et al[30]. In AMD and ASS scenarios, it is hardly possible that iron/sulfide-oxidizing bacteria are not involved in the process of pyrite weathering. Therefore, while the abiotic oxidation research provides a fundamental basis for understanding the role of H_2O_2 in pyrite oxidation, it has some limitations in explaining complex systems involving microbially mediated processes.

We previously examined the oxidation of pyrite cubes that were exposed to an *Acidithiobacillus ferrooxidans* strain (an iron- and sulfide-oxidizing bacterial species commonly present in natural environments), ambient dissolved oxygen and intermittent fluxes of H_2O_2 at micromolar levels under circumneutral (initial pH = 6.8). It was found that Equation 3 did not operate observably due to low Fe^{3+} solubility. The more aggressive nature of H_2O_2 as an oxidant (as compared to molecular oxygen) caused marked surface corrosion of the pyrite cubes. It was observed that cell colonization on the mineral surfaces was inhibited at high H_2O_2 levels (initial concentration of H_2O_2 >100 µmol L^{-1}). However, at a H_2O_2 concentration of 50 µmol L^{-1}, cell attachment was enhanced, as compared to the no-added H_2O_2 treatment[36].

In this article, we report on the experimental results for the acidic scenario (initial pH = 2). This represents a step forward in simulating pyrite weathering involving H_2O_2 in field conditions e.g. pyrite grains in tailings dams, inundated mine waste impoundments and constructed wetlands that receive cyclic flux of micromolar H_2O_2 caused by intermittent rainfall events. Pyrite cubes instead of powdered pyrite were used in this study in order to minimize the possible interference from the spontaneously generated H_2O_2, as reported by Schoonen et al[30], who found that it was a challenge to achieve quantitative measurements of the spontaneously generated H_2O_2. To obtain further insights into the response of planktonic *Acidithiobacillus ferrooxidans* to toxicity of Fenton reaction-derived free radicals and the resulting impacts on the oxidation rate of aqueous Fe^{2+}, a separate experiment was also conducted to observe the evolution of cell population, aqueous Fe^{2+} and other relevant chemical parameters following a single H_2O_2 flux. The objective of this study was to examine the effects of micromolar H_2O_2 flux on the microbially involved oxidation of aqueous Fe^{2+} and cubic pyrite by comparison between the control (no added H_2O_2) and the treatments (with varying dosage levels of H_2O_2) under the same preset experimental conditions.

Results

Aqueous Fe^{2+} oxidation experiments. For the abiotic experiments, the concentration of aqueous Fe^{2+} remained little change when exposed to molecular oxygen only (i.e. the control) for both the low and high Fe^{2+} scenarios. The injection of H_2O_2 (the treatments) caused a sudden decrease in Fe^{2+} within the first 5 min of the experiment. The aqueous Fe^{2+} then maintained at a stable level throughout the entire duration of the experiment after this initial drop. There was a tendency that the magnitude of Fe^{2+} drop increased with increasing dosage level of H_2O_2 (Fig. 1a and c).

In contrast with the abiotic experiment, the concentration of aqueous Fe^{2+} in the control (no added H_2O_2) rapidly decreased in the presence of *Acidithiobacillus ferrooxidans* for both the low and high

Fe^{2+} scenarios (Fig. 1b and d). For the low Fe^{2+} scenario, the initial rapid drop in Fe^{2+} was observed for all the treatments. The aqueous Fe^{2+} evolution patterns in T3 and T4 were similar to those in T3 and T4 of the abiotic experiment, respectively. However, the aqueous Fe^{2+} in T1 and T2 continued to decrease after the initial drop with T1 showing a generally rapider rate of reduction, relative to T2 (Fig. 1b). When the initial concentration of Fe^{2+} in the solutions was increased to 558 mg L^{-1}, there was no significant difference in the aqueous Fe^{2+} evolution pattern among the control, T1 and T2. T3 also had a very similar evolution pattern aqueous Fe^{2+} to the control except that it dropped much quickly during the first 5 min and took a slightly longer time to disappeared in the solution. T4 was the only treatment showing marked delay in aqueous Fe^{2+} depletion (Fig. 1d).

The curves of viable cell population during the incubation experiments for both the low and high Fe^{2+} scenarios are provided in Supplementary Fig. S1a and b. In general, the cell density decreased with increasing dosage level of H_2O_2. Fig. S2 is a selected SEM image showing the cellular damage in the affected microbes.

In the low Fe^{2+} scenario, there was a high degree of similarity in the curves of dissolved oxygen (DO) among the control, T1, T2 and T3. However, T4 showed much higher DO in the earlier stage of the incubation experiment, as compared to the others. This gap was closed at the 40th h of the experiment (Supplementary Fig. S3). The curves of DO were highly consistent among the control and all the treatments for the high Fe^{2+} scenario (data not shown).

Toxic response of *Acidithiobacillus ferrooxidans* to H_2O_2 under various conditions. Figure 2 shows that when the bacteria were exposed to 50 µmol L^{-1} H_2O_2 for 30 min (BH), the cell population in the solution significantly reduced, as compared to the control (BI, without added H_2O_2) and in the treatment (BHA) with a reactive oxygen species scavenger (ascorbic acid), which has the capacity to rapidly decompose H_2O_2. When comparing H_2O_2 only systems (i.e. BH and BIH) with H_2O_2-Fe^{2+} reaction systems (i.e. BIH and BIHA), it can be seen that the cell population was denser in a H_2O_2 only system than in its corresponding H_2O_2-Fe^{2+} system (Fig. 2), indicating that more severe oxidative stress in the cells in the latter than in the former.

Aqueous phase of the pyrite oxidation experiment. The viable cell count on the 6th day after inoculation of *Acidithiobacillus ferrooxidans* was lower than the number of cells added at the time when the inoculum was introduced into the solution for the control and all the treatments. The total number of viable planktonic cells was in the following decreasing order: CP > TP1 = TP2 > TP3 > TP4 on this occasion. Therefore, approximately 35% and 91% of the added bacteria disappeared from the solution for the control and the highest H_2O_2 dosage treatment (TP4), respectively. After this initial drop in planktonic cell population, the number of planktonic cells in various treatments fluctuated with different evolutionary patterns during the period of the incubation experiment. In general, the cell count was higher in CP and TP1 than in the treatments with higher H_2O_2 doses (TP2, TP3 and TP4). TP4 had the lowest cell count at any sampling occasion during the period of the experiment. The cell population in the control and the treatments consistently dropped to the lowest level on the 74th day and remained low until the end of the incubation experiment (Fig. 3a)

On the 3rd day of the experiment, the concentration of aqueous Fe^{2+} was in the following decreasing order: CP > TP4 > TP1 > TP2 > TP3. The Fe^{2+} concentration in TP1, TP2 and TP3 maintained at a level <5 mg L^{-1} during the entire period of the experiment. After the sudden drop from 9.6 mg L^{-1} on the 3rd day to 4.5 mg L^{-1} on the 6th day, the Fe^{2+} concentration in CP also maintained at a level <5 mg L^{-1} for the remaining period of the experiment. In contrast, TP4 exhibited a different Fe^{2+} variation pattern during the period of the experiment; the concentration of Fe^{2+} sharply increased from 8.3 mg L^{-1} on the 3rd day to 26.6 mg L^{-1} and 26.7 mg L^{-1} on the 12th and 15th
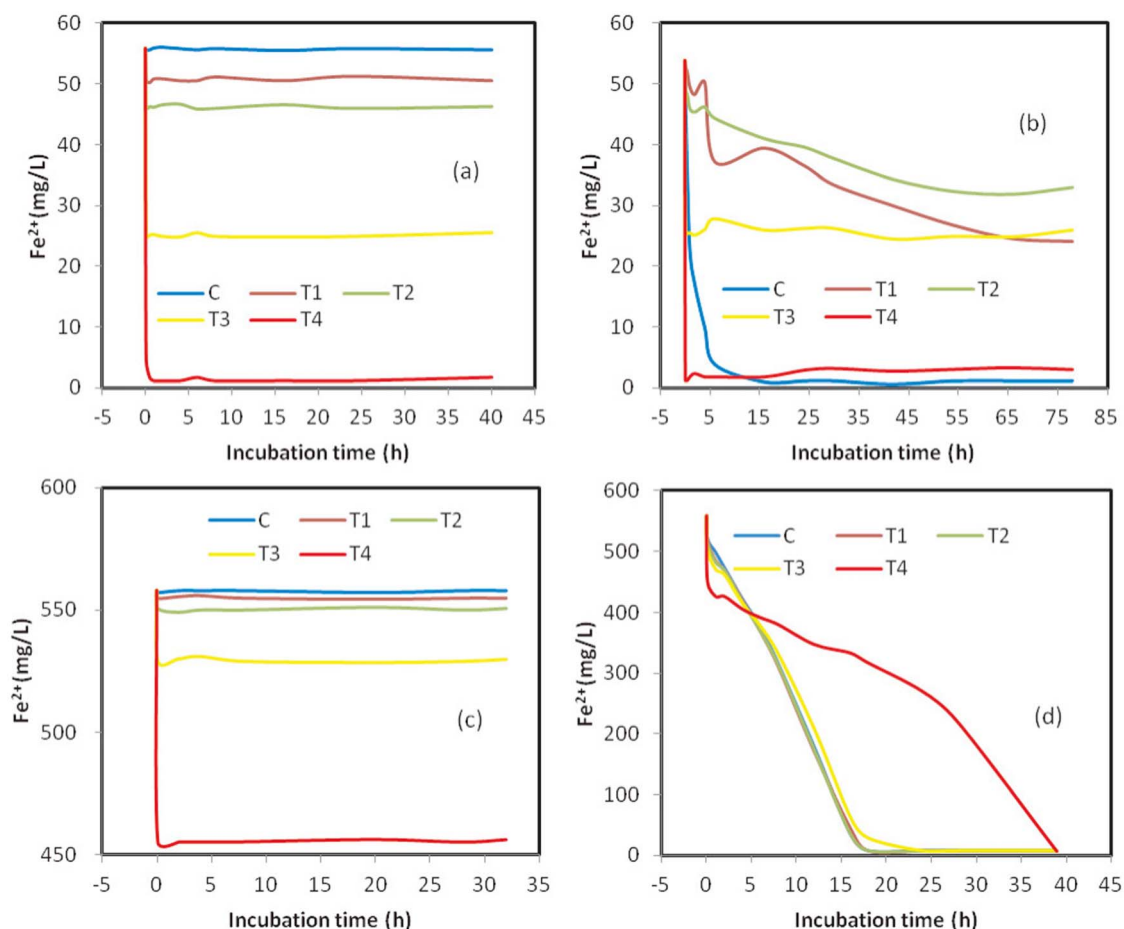
Figure 1 | Evolution of aqueous Fe^{2+} in the solution when exposed to micromolar concentrations of H_2O_2. (a) abiotic oxidation experiment at an initial Fe^{2+} concentration of 55.8 mg L^{-1}, (b) biotic oxidation experiment at an initial Fe^{2+} concentration of 55.8 mg L^{-1}, (c) abiotic oxidation experiment at an initial Fe^{2+} concentration of 558 mg L^{-1}, and (d) biotic oxidation experiment at an initial Fe^{2+} concentration of 558 mg L^{-1}. C: control; T1: 50 μmol L^{-1} H_2O_2; T2: 100 μmol L^{-1} H_2O_2; T3: 300 μmol L^{-1} H_2O_2; and T4: 1000 μmol L^{-1} H_2O_2.

day, respectively and then rapidly decreased to 4.6 mg L^{-1} on the 22nd day; after this, the Fe^{2+} concentration maintained at a level <6 mg L^{-1}, with fluctuation, until the end of the experiment (Fig. 3b).

The aqueous Fe^{3+} had a similar temporal variation pattern for the control and all the treatments, showing a general trend to increase the

Figure 2 | Comparison of cell population among different treatments. *Acidithiobacillus ferrooxidans* were exposed to H_2O_2 (50 μmol L^{-1}) for 30 min. BI: without added H_2O_2; BH: 50 μmol L^{-1} H_2O_2 only; BIH: 50 μmol L^{-1} H_2O_2 and 55.8 mg L^{-1} Fe^{2+}; BHA: 50 μmol L^{-1} H_2O_2 and 50 μmol L^{-1} ascorbic acid; and BIHA: 50 μmol L^{-1} H_2O_2, 55.8 mg L^{-1} Fe^{2+} and 50 μmol L^{-1} ascorbic acid. Error bars represent standard deviation of five replicates.

concentration over time. However, Fe^{3+} concentration in TP4 was always much lower, relative to the control and other treatments on any sampling occasions, and no Fe^{3+} was detected during the initial 19 days of the experiment. In the early part of the experiment, the aqueous Fe^{3+} concentration tended to be markedly higher in CP and TP1 than in TP2 and TP3. However, this gap was gradually reduced in the latter part of the experiment (Fig. 3c).

There was a clear tendency that the aqueous sulfur concentration increased with increasing incubation time. This was accompanied by an opposite trend for the solution pH. Closer examination found that on most sampling occasions, TP4 had a higher pH and lower S concentration, as compared to the control and other treatments (Fig. 3d and e).

Scanning electron microscope (SEM) observations and X-ray photoelectron spectroscopy (XPS) analysis of the pyrite cube surfaces. No attached cells were observed on the surface of pyrite cubes that were taken on the 28th day of the experiment for the control and various treatments. Pitting corrosion was clearly observable for CP and TP1 but not for other treatments (Fig. 4a, d, g, j and m). The micro-morphological features of the reacted pyrite surfaces were markedly different at the end of the experiment, as compared with those observed on the 28th day. Except for TP4, all the treatments and the control exhibited marked surface cracking and partially flaking corrosion (Fig. 4b, e, h, k and n). Attached cells were clearly observed to occur on the flakes that were still tightly or loosely attached to the pyrite substrate for TP1, TP2 and TP3 (Fig. 4f, i and l). Scattered cell-shaped objects were also observed on the
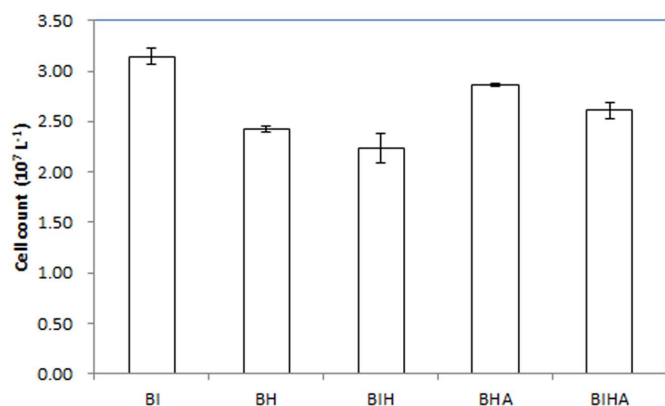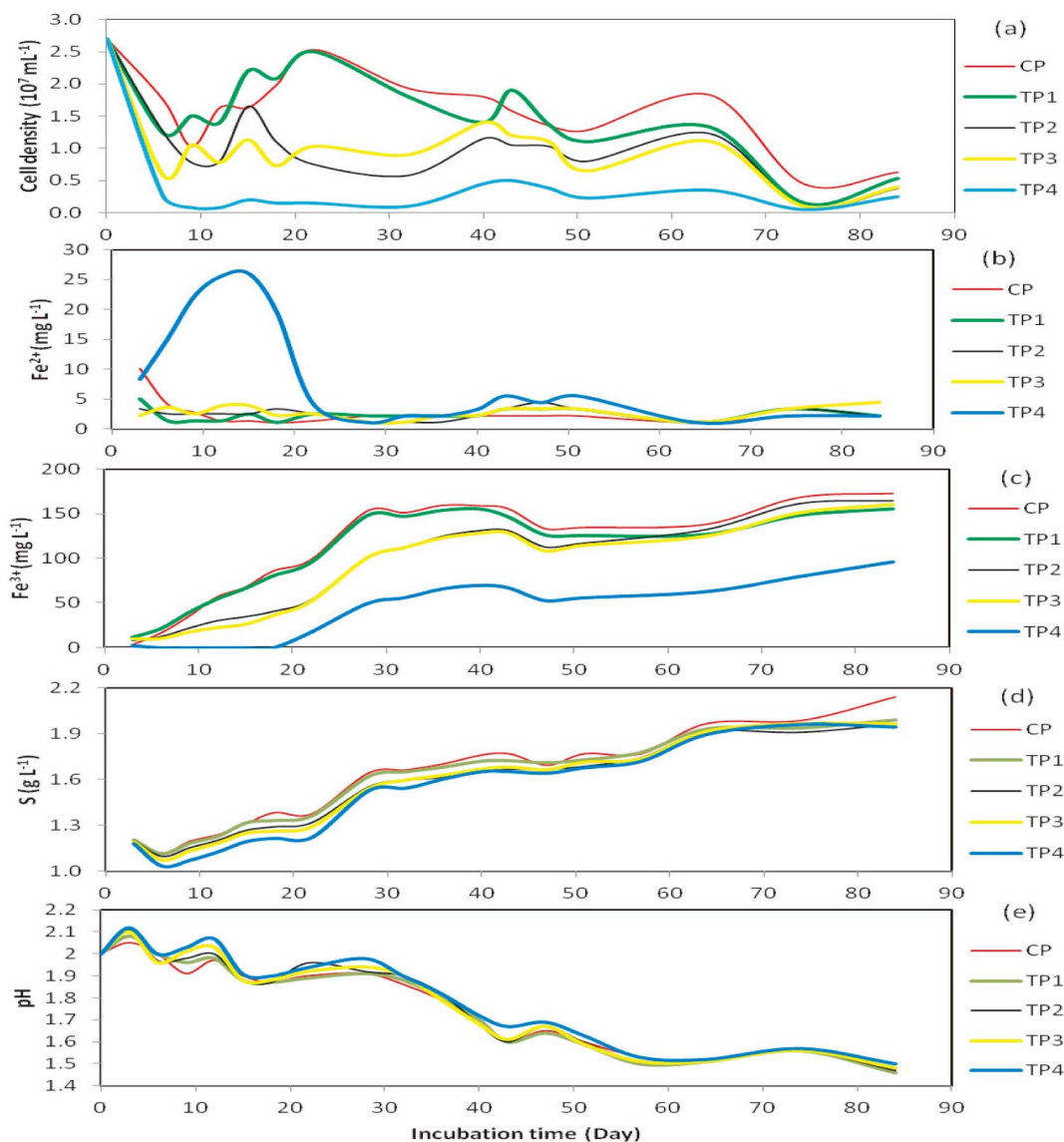
3

Figure 3 | Changes in (a) planktonic cell population, (b) ferrous ion concentration, (c) ferric ion concentration, (d) sulfur concentration, and (d) pH in the solution during the period of incubation experiment for the control and various treatments.

mineral surfaces for CP and TA4 (Fig. 4c and o), but they were not as clear as those observed for TP1, TP2 and TP3.

The XPS results showed that within a ~3–5 nm thick surface layer of the reacted mineral surface, oxygen accounted for a large proportion (52–79% on a molar basis) of the sum of iron, sulfur and oxygen. There was a trend that the oxygen percentage decreased with increasing dosage level of H_2O_2 in the solution (Fig. 5a). The Fe/S ratio of the reacted surfaces ranged from 0.183 to 0.257, which was much lower than the value (0.5) of the theoretical Fe/S ratio for pyrite. After treatment of the reacted pyrite cubes with the boiling HCl to remove the oxidized materials, the proportion of oxygen in the sum of iron, sulfur and oxygen markedly decreased for the outermost layer (top ~3–5 nm thick) of the corroded surface (Fig. 5b). The Fe/S ratio of the corroded surface ranged from 0.173 to 0.239, which was not markedly different from those prior to HCl treatment.

There was a trend that XPS peaks of Fe $2p_{3/2}$ and S $2p$ shifted to lower binding energies with increasing dosage level of H_2O_2, indicating that higher level of H_2O_2 resulted in increased proportion of lower-valence species of Fe and S on the reacted pyrite surfaces (Table 1). CP and TP1 exhibited the dominance of Fe^{3+} (in Fe-OH bond) in the surface Fe species. There was a trend that the percentage

of Fe^{3+} decreased with increasing H_2O_2 level. Fe^{2+} (in Fe-S bond) was not detected for CP and TP1but dominated the surface Fe species for TP2, TP3 and TP4. In agreement with surface Fe speciation, S^- dominated the surface S species for TP2, TP3 and TP4 while CP and TP1 only contained small amount of surface S^-. The percentage of surface sulfate-S was greater in CP and TP1 than in TP2, TP3 and TP4. Small amount of thiosulfate-S was also detected for CP and TP1.

After HCl treatment, the chemical states of Fe and S were highly consistent among the control and the treatments, showing the predominant presence of surface Fe^{2+} and S^- (in Fe-S bond). Polysulfides with varying valences (including the end product elemental S) were also present at significant amounts. Trace amounts of monosulfide (S^{2-}) were also detected. Fe^{2+}/Fe^{3+} (in Fe-O/Fe-S bonds) accounted for about 34% ($\pm$3%) (Table 2).

Discussion

In the presence of dissolved oxygen alone (the control), no clear sign of Fe^{2+} oxidation was observed. This is consistent with the established theory that oxidation of aqueous Fe^{2+} by molecular oxygen under acidic pH was kinetically slow[3]. Consequently, the sudden drop in aqueous Fe^{2+} concentration for the treatments with the
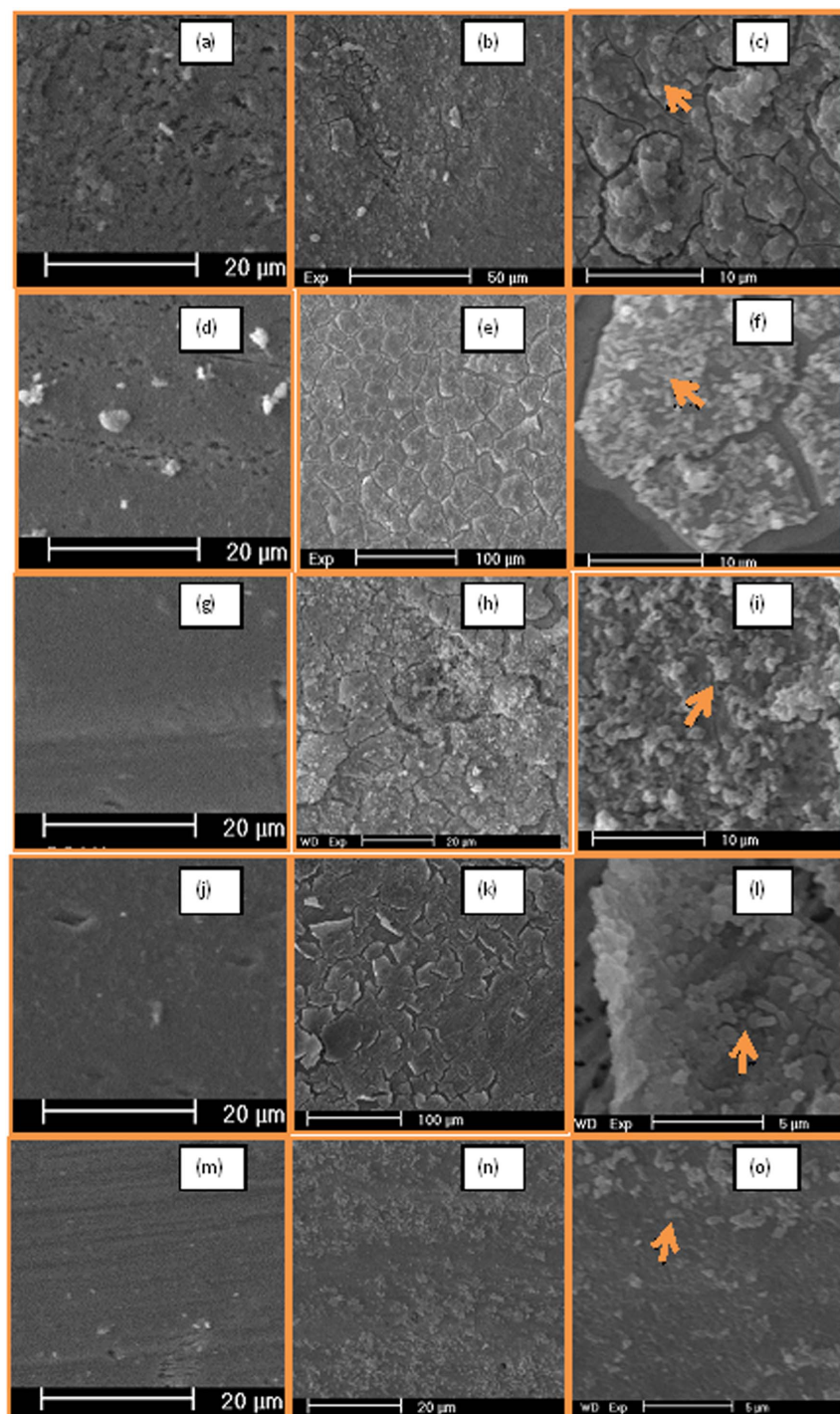
4

Figure 4 | SEM images showing the micro-morphological characteristics of the reacted surfaces of pyrite cubes taken on the 28th day of the experiment. (a) control (CP), (d) TP1, (g) TP2, (j) TP3, and (m) TP4; pyrite cubes taken at the end of the experiment (the 86th day): (b) control (CP), (e) TP1, (h) TP2, (k) TP3, and (n) TP4; (f), (i) and (l) show the presence of attached cell clusters on the reacted mineral surfaces (the 86th day) for TP1, TP2 and TP3, respectively and the arrows point to such example clusters in these three treatments; (c) and (o) point to the scattered cell-shaped objects on the reacted mineral surfaces (the 86th day) for the control (CP) and TP4, respectively.

added H_2O_2 can be interpreted as the result of H_2O_2-driven oxidation of aqueous Fe^{2+}. The "standstill" of aqueous Fe^{2+} level after this initial rapid oxidation indicates that the H_2O_2 was already depleted within a few minutes. The rapid consumption of H_2O_2 through Fe^{2+} oxidation can be expressed by the following chemical equations:

$$Fe^{2+} + H_2O_2 \rightarrow Fe^{3+} + HO^{\bullet} + OH^- \qquad (4)$$

$$Fe^{2+} + HO^{\bullet} \rightarrow Fe^{3+} + OH^- \qquad (5)$$
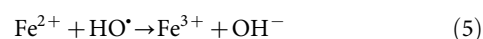
The decomposition of 1 mole of H_2O_2 leads to simultaneous oxidation of 1 mole of Fe^{2+} and generation of 1 mole of $HO^{\bullet}$ (Equation 4), which may further oxidize another mole of Fe^{2+} (Equation 5). If spontaneous decomposition of H_2O_2 takes place, elevated concentration of DO is expected according to the following equation:
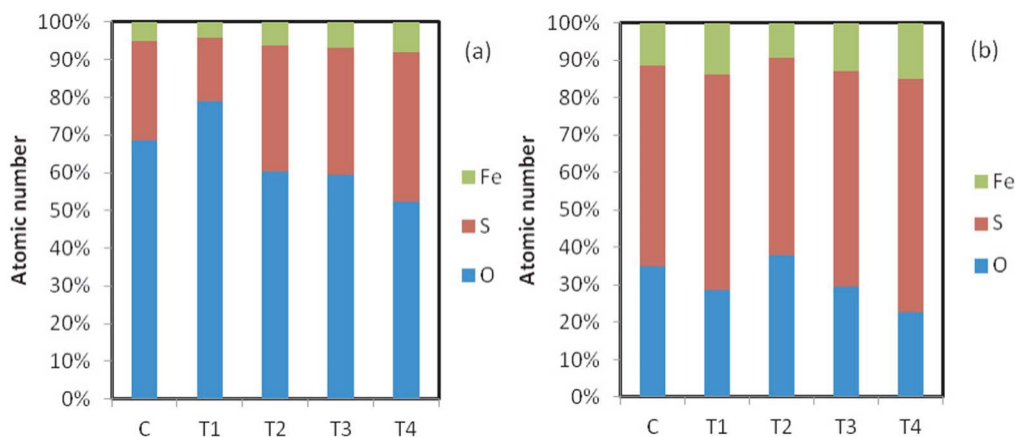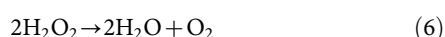
Figure 5 | Comparison of chemical composition (normalized to oxygen, sulfur and iron) in (a) the reacted pyrite cube surface and (b) the corroded pyrite cube surface among the control and various treatments.

$$2H_2O_2 \rightarrow 2H_2O + O_2 \qquad (6)$$

The trend lines showing the evolution of DO were very similar among the control and T1–T3 for the low Fe^{2+} scenario, indicating that spontaneous decomposition of H_2O_2, if any, was not significant for these treatments (Supplementary Fig. S3). The higher DO in T4 suggests that spontaneous decomposition of H_2O_2 did occur for this high-dose treatment. This is supported by the fact that the ratio of the converted Fe^{2+} to H_2O_2 was less than 1, indicating that over half of the added H_2O_2 was not consumed through Fe^{2+} oxidation.

By comparison with the abiotic oxidation results, it is evident that microbes played a crucial role in further oxidation of aqueous Fe^{2+} following the initial H_2O_2-driven oxidation in the corresponding biotic systems. However, the ability of microbes to catalyze the oxidation of aqueous Fe^{2+} was markedly affected by the initial concentration of aqueous Fe^{2+}. When the initial concentration of aqueous Fe^{2+} was 55.8 mg L^{-1}, the microbially mediated Fe^{2+} oxidation was impeded for all the treatments, as compared to the control. The oxidation rate of aqueous Fe^{2+} tended to decrease with increasing dose of H_2O_2. This was consistent with the observed decrease in cell population and cellular damage in the affected microbes (Supplementary Fig. S1a and Fig. S2) in response to the toxicity of hydroxyl radical that was generated through Fenton reaction (Equation 4). As shown in Fig. 2, H_2O_2 at an initial concentration of 50 μmol L^{-1} could cause marked oxidative stress in the cells. However, the presence of hydroxyl radical did increase the degree of oxidative stress in the cells.

In comparison with the low initial aqueous Fe^{2+} scenario (55.8 mg L^{-1}), the microbial oxidation of aqueous Fe^{2+} was not retarded for the treatments except for T4 (H_2O_2 at 1000 μmol L^{-1}) when the initial concentration of aqueous Fe^{2+} was increased to 558 mg L^{-1}. The reduced microbial toxicity level due to the presence of higher initial concentration of aqueous Fe^{2+} can be attributed to the effect of excessive Fe^{2+} on scavenging $HO^{\bullet}$, as shown in Equation 5.

Rapid disappearance of most added *Acidithiobacillus ferrooxidans* from the nutrient solution containing powdered pyrite was observed and attributed to the colonization of the bacteria on the pyrite mineral surfaces[37,38]. However, the lack of evidence showing the presence of attached cells and cell-shaped corrosion pits on the surfaces of pyrite cubes taken on the 28th day of the experiment suggests that this was not the case in this study. The general trend that the viable planktonic cell population decreased with increasing H_2O_2 dosage level suggests that the H_2O_2-derived $HO^{\bullet}$ resulted in the growth inhibition or even killing of some *Acidithiobacillus ferrooxidans* following inoculation. Ferrous ion was present in all the solutions at least after the 3rd day of the experiment. Consequently, free radical generation was possible.

Table 1 | Chemical state of iron and sulfur on the reacted surfaces of pyrite. BE and At% denote binding energy and atomic percentage, respectively. Peak assignment was done by comparison with literature values (Table S1 in the Supplementary Information)

	Peak	BE (eV)	Species	At%
Fe $2p_{3/2}$				
C	a	708.6	Fe^{2+}/Fe^{3+} (Fe-O/Fe-S)	43.5
	b	709.1	Fe^{3+} (Fe-S)	12.7
	c	712.3	Fe^{3+} (Fe-OH)	43.8
T1	a	708.9	Fe^{2+}/Fe^{3+} (Fe-O/Fe-S)	3.2
	b	708.9	Fe^{2+}/Fe^{3+} (Fe-O/Fe-S)	38.2
	c	712.0	Fe^{3+} (Fe-OH)	58.7
T2	a	707.1	Fe^{2+} (Fe-S)	46.4
	b	707.6	Fe^{2+} (Fe-S)	18.6
	c	711.0	Fe^{3+} (Fe-O/Fe-OH)	35.0
T3	a	707.3	Fe^{2+} (Fe-S)	63.5
	b	708.3	Fe^{2+}/Fe^{3+} (Fe-O/Fe-S)	18.9
	c	711.2	Fe^{3+} (Fe-OH)	17.6
T4	a	707.2	Fe^{2+} (Fe-S)	58.3
	b	708.7	Fe^{2+}/Fe^{3+} (Fe-O/Fe-S)	33.9
	c	711.7	Fe^{3+} (Fe-OH)	7.8
S 2p				
C	a	163.1	S°	6.6
	b	163.9	S_n^{-}/S°	48.1
	c	165.1	S_n^{-}/S°	33.4
	d	166.2	S^{2+} ($S_2O_3^{2-}$)	1.8
	e	169.7	S^{6+} (SO_4^{2-})	10.1
T1	a	162.3	S^{-}	2.8
	b	163.6	S_n^{-}/S°	10.3
	c	164.3	S_n^{-}/S°	43.8
	d	165.5	S_n^{-}/S°	27.5
	e	166.6	S^{2+} ($S_2O_3^{2-}$)	1.7
	f	169.9	S^{6+} (SO_4^{2-})	14.0
T2	a	161.6	S^{2-}	4.3
	b	162.6	S^{-}	53.3
	c	163.7	S_n^{-}/S°	34.6
	d	164.8	S_n^{-}/S°	1.6
	e	168.3	S^{6+} (SO_4^{2-})	6.2
T3	a	161.6	S^{2-}	3.4
	b	162.7	S^{-}	58.5
	c	163.8	S_n^{-}/S°	30.1
	d	164.6	S_n^{-}/S°	4.3
	e	168.5	S^{6+} (SO_4^{2-})	3.7
T4	a	161.6	S^{2-}	2.2
	b	162.6	S^{-}	47.1
	c	163.7	S_n^{-}/S°	23.2
	d	164.1	S_n^{-}/S°	19.8
	e	168.6	S^{6+} (SO_4^{2-})	7.7

Table 2 | Chemical state of iron and sulfur on the corroded surfaces of pyrite. BE and At% denote binding energy and atomic percentage, respectively. Peak assignment was done by comparison with literature values (Table S1 in the Supplementary Information)

	Peak	BE (eV)	Species	At%
Fe 2p3/2				
C	a	707.1	Fe^{2+} (Fe-S)	63.3
	b	708.1	Fe^{2+}/Fe^{3+} (Fe-O/Fe-S)	36.7
T1	a	707.2	Fe^{2+} (Fe-S)	66.4
	b	708.5	Fe^{2+}/Fe^{3+} (Fe-O/Fe-S)	33.6
T2	a	707.2	Fe^{2+} (Fe-S)	65.2
	b	708.0	Fe^{2+}/Fe^{3+} (Fe-O/Fe-S)	34.8
T3	a	707.2	Fe^{2+} (Fe-S)	69.0
	b	708.2	Fe^{2+}/Fe^{3+} (Fe-O/Fe-S)	31.0
T4	a	707.1	Fe^{2+} (Fe-S)	62.8
	b	708.0	Fe^{2+}/Fe^{3+} (Fe-O/Fe-S)	37.2
S 2p				
C	a	161.6	S^{2-}	2.6
	b	162.5	S^{-}	46.8
	c	163.6	S_n^{-}/S°	29.1
	d	163.7	S_n^{-}/S°	21.4
T1	a	161.7	S^{2-}	3.6
	b	162.6	S^{-}	52.4
	c	163.8	S_n^{-}/S°	24.6
	d	164.1	S_n^{-}/S°	19.4
T2	a	161.6	S^{2-}	4.0
	b	162.6	S^{-}	52.9
	c	163.7	S_n^{-}/S°	24.6
	d	164.0	S_n^{-}/S°	18.5
T3	a	161.6	S^{2-}	3.6
	b	162.6	S^{-}	54.9
	c	163.7	S_n^{-}/S°	26.4
	d	164.1	S_n^{-}/S°	15.1
T4	a	161.5	S^{2-}	2.6
	b	162.5	S^{-}	50.9
	c	163.6	S_n^{-}/S°	23.3
	d	163.7	S_n^{-}/S°	23.3

However, it cannot be excluded that insufficient supply of Fe^{2+} to feed all the bacteria also contributed to the decrease in the viable planktonic cell population during the initial stage of the experiment[39]. This explains the initial drop in planktonic cell count for the control, which contained no added H_2O_2.
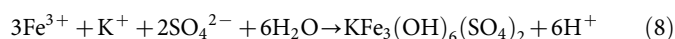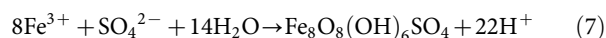
The marked recovery of the bacterial population after the initial drop for CP and TP1 can be attributed to (a) the adaptation of the bacteria to the H_2O_2-induced oxidative stress, (b) the increased supply of Fe^{2+} released from the mineral surfaces, and (c) possibly, the reduced concentration of free radicals as a result of the increased release rate of Fe^{2+}, which alleviated the oxidative stress in *Acidithiobacillus ferrooxidans*, as discussed above.

The decreasing trend in cell density at the later stage of the experiment for CP and TP1 was likely to be caused by the reduced rate of Fe^{2+} release from the mineral surface during this period (the reasons for this have been discussed previously), as evidenced by the low concentration of aqueous Fe^{2+} and negative to very slow increase in aqueous Fe^{3+} during the period from the 28th day to the end of the experiment. This made the solutions become less and less favourable for the growth of the planktonic bacteria. Consequently, the bacteria had to seek alternative "food" sources by landing on the mineral surfaces and feeding on the sulfur-rich substrates. This is in contrast with the scenario at the earlier stage of the experiment (excluding the initial 6 days) when sufficient amount of Fe^{2+} was constantly released into the solution. The results obtained here indicates that the *Acidithiobacillus ferrooxidans* preferentially fed on free Fe^{2+} and
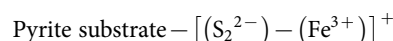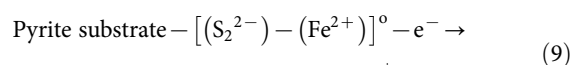
possibly thiosulfate ($S_2O_3^{2-}$) in the solution rather than the structurally bound Fe^{2+} and reduced S species.
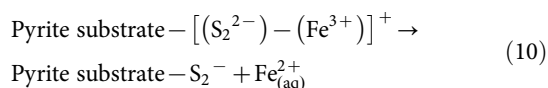
The absence of Fe^{3+} in TP4 until the 19th day of the experiment indicates that Fe^{2+} oxidation was negligible during this period. This resulted in the accumulation of Fe^{2+} in the solution. Clearly, the weak microbial activity resulting from the high dosage level of H_2O_2 was responsible for the inhibition of Fe^{2+} oxidation while the H_2O_2 itself as an oxidant had limited effect on the abiotic oxidation of the aqueous Fe^{2+} under the set experimental conditions. The aqueous Fe^{3+} concentration reflected the combined effect of the Fe^{3+} production from Fe^{2+} oxidation and the Fe^{3+} immobilization due to precipitation of iron compounds (precipitates were observed during the experiment but they were not produced in sufficient quantity to allow chemical and mineralogical analysis). Therefore, the steady increase in aqueous Fe^{3+} in CP and TP1 until the 28th day of the experiment indicates a higher rate of the Fe^{2+}-Fe^{3+} conversion, relative to the rate of Fe^{3+} immobilization during this period. This more or less corresponded with a period when the bacterial population rapidly increased, reflecting an interdependency relationship between the Fe^{2+}-Fe^{3+} conversion rate and the bacterial density. The subsequent plateau and decline phase of aqueous Fe^{3+} evolution was likely to represent a period of reduction in Fe^{3+} production as a result of reduced rate of Fe^{2+} release. This can be supported by the fact that the bacterial population tended to decrease during this period. The high similarity of Fe^{3+} evolutionary pattern between CP and TP1 suggests that a H_2O_2 level of 50 µmol L^{-1} was unlikely to cause a marked reduction in microbial oxidation of aqueous Fe^{2+} under the set experimental conditions. However, the increased dosage level of H_2O_2 tended to result in lower Fe^{3+} concentration in the solution. It is interesting to note that the Fe^{2+} concentration remained low during the entire period of the experiment for the H_2O_2 treatments except for the earlier stage of TP4. This indicates that the Fe^{2+}-Fe^{3+} conversion rate more or less kept pace with the Fe^{2+} production rate. Therefore, the reduced rate of Fe^{2+} release from the mineral surface was a more upstream cause responsible for the lower solution Fe^{3+} concentration in these treatments.

The molar ratio of Fe to S in the solution ranged from 0.15 to 0.22, which were much smaller than the theoretical value of 0.5 assuming that equal amount of Fe and S was liberated from the pyrite cube surfaces during the experiment. In fact, it was likely that more Fe than S entered into the solution during the experiment, as evidenced by the presence of the Fe-deficient reacted pyrite surfaces (Fig. 5a). Therefore, much more Fe than S was removed from the solution through iron compound precipitation. Schwertmannite ($Fe_8O_8(OH)_6SO_4$) and jarosite ($KFe_3(OH)_6(SO_4)_2$) have a Fe/S molar ratio of 8 and 1.5, respectively. Therefore, the formation of basic sulfate minerals such as schwertmannite and jarosite explains the imbalance between Fe and S in the solution. This is consistent with the observed generation of H^+ (as indicated by pH drop) as a result of Fe^{3+} hydrolysis leading to the formation of these minerals:

$$8Fe^{3+} + SO_4^{2-} + 14H_2O \rightarrow Fe_8O_8(OH)_6SO_4 + 22H^+ \quad (7)$$

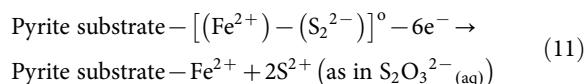$$3Fe^{3+} + K^+ + 2SO_4^{2-} + 6H_2O \rightarrow KFe_3(OH)_6(SO_4)_2 + 6H^+ \quad (8)$$

The Fe-deficient nature of the corroded surfaces (after HCl treatment to remove the coatings) indicates that the pyrite-Fe was preferentially liberated from the mineral surface, as compared to the pyrite-S. This can be explained by the relative easiness of the pyrite-Fe liberation reaction, as shown in the following chemical equations:
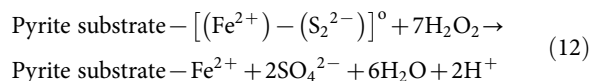
$$
\begin{aligned}
&\text{Pyrite substrate} - \left[(S_2^{2-}) - (Fe^{2+})\right]^{\circ} - e^- \rightarrow \\
&\text{Pyrite substrate} - \left[(S_2^{2-}) - (Fe^{3+})\right]^{+}
\end{aligned} \quad (9)
$$

$$\text{Pyrite substrate} - \left[\left(S_2{}^{2-} \right) - \left(Fe^{3+} \right) \right]^{+} \rightarrow$$
$$\text{Pyrite substrate} - S_2{}^{-} + Fe^{2+}_{(aq)} \tag{10}$$

The completion of the above chemical reactions requires only one electron transfer from pyrite-Fe^{2+} to an electron acceptor (oxidant) in the solution, leaving structurally bound polysulfides ($S_2{}^{-}$) on the mineral surfaces. In contrast, the liberation of pyrite-$S_2{}^{2-}$ requires multiple steps of electron transfer from the pyrite surface to electron acceptors. The minimum number of electrons needed to be transferred to the external oxidants in order to liberate two pyrite-S atoms is 6 according to the equation below:
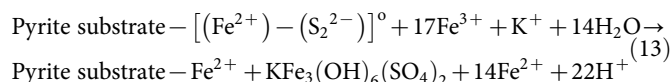
$$\text{Pyrite substrate} - \left[\left(Fe^{2+} \right) - \left(S_2{}^{2-} \right) \right]^{o} - 6e^{-} \rightarrow$$
$$\text{Pyrite substrate} - Fe^{2+} + 2S^{2+} \left(\text{as in } S_2O_3{}^{2-}{}_{(aq)} \right) \tag{11}$$

Consequently, the oxidation of pyrite-$S_2{}^{2-}$ did not keep pace with the oxidation of pyrite-Fe^{2+}, leaving sulfur species of intermediate oxidation states remained structurally connected with the pyrite substrate. The presence of a surfur-rich surface layer in oxidized pyrite crystals was also observed by others[40,41].

The XPS results indicate the presence of oxidation products containing Fe^{3+} and $SO_4{}^{2-}$ within the ~3–5 nm thick outermost layer of the reacted pyrite surface. This suggests the formation of coating materials such as ferric (oxy)hydroxysulfates and (oxy)hydroxides. Xia et al[42] observed the presence of jarosite in the microbially oxidized pyrite surfaces at acidic pH and suggested that the formation of surface-jarosite was the major cause responsible for the passivation of the sulfide mineral surfaces. The tendency that the proportion of surface-Fe^{3+} and -$SO_4{}^{2-}$ decreased with increasing dosage level of H_2O_2 appears to suggest that the presence of H_2O_2 affected the build-up of the ferric (oxy)hydroxysulfate-containing coating layer on the mineral surfaces although the exact mechanisms are not clear. Possibly, the differential composition of oxidants in the different H_2O_2-treated systems was an upstream factor that needs to be considered for the interpretation of the observed phenomena. From CP to TP4, the relative importance of H_2O_2-driven surface oxidation was likely to increase as a result of the increase in the H_2O_2 concentration and the simultaneous decrease in Fe^{3+} concentration. The weakened role of Fe^{3+} as a driving oxidant for mineral surface oxidation might reduce the frequency of Fe^{3+}-$SO_4{}^{2-}$ contact at the solution-mineral interfaces, and consequently disfavour the formation of ferric (oxy)hydroxysulfate coatings, as described by the following H_2O_2-driven oxidation reaction:

$$\text{Pyrite substrate} - \left[\left(Fe^{2+} \right) - \left(S_2{}^{2-} \right) \right]^{o} + 7H_2O_2 \rightarrow$$
$$\text{Pyrite substrate} - Fe^{2+} + 2SO_4{}^{2-} + 6H_2O + 2H^{+} \tag{12}$$

This is in contrast with the Fe^{3+}-driven oxidation reaction, as shown in the following equation describing the formation of jarosite:

$$\text{Pyrite substrate} - \left[\left(Fe^{2+} \right) - \left(S_2{}^{2-} \right) \right]^{o} + 17Fe^{3+} + K^{+} + 14H_2O \rightarrow$$
$$\text{Pyrite substrate} - Fe^{2+} + KFe_3(OH)_6(SO_4)_2 + 14Fe^{2+} + 22H^{+} \tag{13}$$

Since no surface-S^{-} was detected by XPS for CP and TP1, it is reasonable to believe that the thickness of the coating layer on the pyrite cube surfaces was >3–5 nm when the mineral crystals were exposed to H_2O_2 at a dosage level below 50 μmol L^{-1}. The coating layer became thinner with increasing dosage level of H_2O_2, resulting in the occurrence of bulk pyrite-S (S^{-}) within the ~3–5 nm thick outermost layer of the original reacted pyrite surfaces, which was consistent with the XPS results for the treatments with high H_2O_2 doses.

The research findings obtained from this study shed some light on the possible complication of the biogeochemical processes associated with the weathering of pyrite and other sulfide minerals due to the presence of H_2O_2 in the concentration range that may be encountered in field conditions. Our recent work[43] also suggests that the Fe^{2+}-H_2O_2 combinations that are likely to be encountered in natural waters resulted in significant degradation of agricultural herbicides. There is, therefore, a strong rationale for conducting additional laboratory-based investigations to obtain further insights into the exact chemical mechanisms and kinetics, and the subsequent field-scale study, which can be used to better evaluate the environmental risk of the toxic surface runoff from acid sulfate soils and sulfidic mine sites, and develop cost-effective management strategies and techniques to minimize its environmental impacts.

Methods

Pyrite specimens and pretreatment. The pyrite specimens used in this study were natural pyrite cubes purchased from the Anhui Tongling Siling Mineral Ltd. For this study, the purpose was to examine the effects of externally originated H_2O_2 on microbially involved oxidation of aqueous Fe^{2+} and pyrite grain surfaces. Therefore, powdered pyrite with high specific surface area was not appropriate due to its potential for causing the production of spontaneous H_2O_2[30]. Pyrite cubes with similar size (approximately $1.5 \times 1.5 \times 1.5$ cm^3) were selected for the mineral-solution contact experiment. Pyrite surfaces are readily reactive when exposed to air. Pyrite oxidation products are expected to be present on the surfaces of any naturally occurring pyrite specimens. It is necessary to remove these coating materials prior to pyrite oxidation experiment. The surfaces of the mineral crystals were treated with a boiling 6 mol L^{-1} HCl solution to remove any oxides, (oxy)hydroxides and (oxy)hydroxysulfates of iron that were possibly present on the original mineral surfaces[44]. The "cleaned" pyrite cubes were immediately used for the experiment after washing with distilled water twice and acetone for three times to further remove elemental sulfur that is possibly present on the mineral surfaces.

Bacteria, culture conditions and inoculum preparation. A strain of *Acidithiobacillus ferrooxidans* was purchased from the China Marine Microbial Culture Collection Center (MCCC). The bacterial culture was maintained at 4°C in a 9 K nutrient medium[39] containing 3.0 g of $(NH_4)_2SO_4$, 0.01 g of $Ca(NO_3)_2$, 0.5 g of $MgSO_4.7H_2O$, 0.5 g of K_2HPO_4, 0.1 g of KCl and 44.3 g of $FeSO_4.7H_2O$ in 1 L of distilled water with pH adjusted to 1.6 with a H_2SO_4 solution.

The inoculum was prepared prior to the experiment. An adequate amount of the bacteria required for the experiment was produced by facilitating bacterial growth in a sterile 9 K medium at 30°C, coupled with shaking (130 rpm) on a rotary shaker for 5–6 days. The cells in the enriched suspension were firstly separated from the iron precipitates (formed during the incubation) by centrifugation at 3000 rpm for 3 min to allow the settlement of the solid iron compounds. The cells remained in the suspension were then transferred into a new centrifuge tube and harvested by centrifugation at 5000 rpm for 10 min to allow the settlement of the cells. After washing twice with sterile distilled water (adjusted to pH 2 with a H_2SO_4 solution), the inoculum was formed by adding an appropriate amount of the same acidified distilled water into the centrifuge tube containing the cleaned cells. The cell concentration in the inoculum for each batch was determined by direct cell counting prior to addition of the inoculum into the experimental reactors in an experiment.

Aqueous Fe^{2+} oxidation experiment. Both biotic and abiotic experiments were conducted to observe the oxidation of Fe^{2+} following a single injection of H_2O_2. The abiotic experiment was to account for the effect of H_2O_2 as an oxidant on the chemical oxidation of aqueous Fe^{2+} while the biotic experiment was to examine the integrative effects of H_2O_2 (as an oxidant and a toxicant to iron-oxidizing bacteria) on Fe^{2+} oxidation. One control (C, without added H_2O_2) and four treatments with different initial H_2O_2 concentrations were established: (a) Treatment 1 (T1): 50 μmol L^{-1}; (b) Treatment 2 (T2): 100 μmol L^{-1}; (c) Treatment 3 (T3): 300 μmol L^{-1}; and (d) Treatment 4 (T4): 1000 μmol L^{-1}. For either biotic or abiotic experiment, two separate experiments with different initial levels of Fe^{2+} were conducted: (a) 55.8 mg L^{-1} and (b) 558 mg L^{-1}.

For all the experiments, a Fe-free 9 K medium (without added $FeSO_4 \cdot 7H_2O$) was used as the basal solution (*i.e.* the solution prior to the addition of various ingredients). A 150 mL conical flask was used as a batch reactor to contain 100 mL of a reacting solution with a pre-set H_2O_2-Fe^{2+} combination. The pH of the reacting medium was adjusted to 2 using a H_2SO_4 solution.

For the biotic experiments, the reacting medium was inoculated with *Acidithiobacillus ferrooxidans* at an initial cell concentration of 1.1×10^7 cells mL^{-1} for the lower Fe^{2+} treatments and 1.0×10^7 cells mL^{-1} for the higher Fe^{2+} treatments. All the conical flasks were loosely wrapped by aluminum foil to allow entry of air but not dust during the entire period of the experiment except at the time of sample collection. The reactors were shaken at 130 rpm on a rotary shaker with temperature set at 30°C. A small amount of sample was taken at different time to determine residual Fe^{2+} concentration, cell density and other relevant parameters. The experiment was performed in triplicate.

For the abiotic experiments, DO in the solutions was also monitored to examine whether marked spontaneous decomposition of H_2O_2 took place during the incubation experiment according to Equation 6.

Pre-experiment tests indicated that the added H_2O_2 was almost depleted within 5 min in the reaction systems investigated for the current study. Consequently,

monitoring of H_2O_2 was not performed due to the following reasons: (a) the research objective (overall effects of H_2O_2 flux at the preset initial concentrations on the microbial oxidation of cubic pyrite and aqueous Fe^{2+}) can be satisfactorily achieved without knowing the detailed evolution of H_2O_2 within the 5 min following the H_2O_2 injection; (b) the measured values of H_2O_2 for the different treatments are not reasonably comparable for such highly dynamic reaction systems since it is technically very difficult, if not impossible, to ensure the simultaneous analysis for the samples of all the treatments; and (c) there is a lack of highly reliable analytical methods for rapid measurements of micromolar level H_2O_2[30].

Pyrite oxidation experiment. The basal solution used was the same as the aqueous Fe^{2+} oxidation experiment. The "cleaned" pyrite cubes were exposed to H_2O_2 at various initial concentrations in the basal solution (with the pH adjusted to 2.0 by a H_2SO_4 solution) in the presence of the *Acidithiobacillus ferrooxidans* at an initial concentration of 2.7×10^7 cells mL^{-1}. One control (CP, without added H_2O_2) and four treatments with different initial H_2O_2 concentrations were established: (a) Treatment1 (TP1): 50 $\mu mol\,L^{-1}$; (b) Treatment 2 (TP2): 100 $\mu mol\,L^{-1}$; (c) Treatment 3 (TP3): 300 $\mu mol\,L^{-1}$; and (d) Treatment 4 (TP4): 1000 $\mu mol\,L^{-1}$. A 250 mL conical flask was used as the reaction chamber. Five pyrite cubes were soaked in 90 mL of a respective solution for the control and each treatment. The conical flask was loosely wrapped using aluminium foil to allow entry of air but not dust and then kept in a biological incubator with the temperature set at $30°C$ during the entire period of the experiment except at the time of cyclic H_2O_2 injection and sample collection.

A time interval of 3–5 days was established for re-injection of H_2O_2, in-situ measurements of pH and solution sample collection for determinations of Fe^{2+}, total Fe, S and cell density. After sampling, an equal amount of sterile Fe-free 9 K medium was added into the reactor to compensate the solution loss caused by the sample collection. To avoid markedly disturbing the solution equilibrium system, the volume of solution samples for chemical and microbial monitoring had to be minimized. Therefore only the above important parameters were measured for this experiment.

The experiment lasted for 86 days. On the 28th day of the experiment, two of the five pyrite cubes for the control and each treatment were taken for surface characterization analysis: one was used for observing the original oxidized surface and another was treated with a boiling 6 $mol\,L^{-1}$ HCl solution to remove the oxidized materials for observing the corroded surface. At the end of the experiment, the pyrite cubes were harvested for surface characterization analysis to compare with those collected on the 28th day of the experiment.

Toxic response of *Acidithiobacillus ferrooxidans* to H_2O_2 under various conditions. Because both aqueous Fe^{2+} and cubic pyrite oxidation experiments indicated that *Acidithiobacillus ferrooxidans* experienced stress when exposed to H_2O_2, a supplementary toxic response experiment was conducted to determine whether the bacterial oxidative stress was caused by H_2O_2 alone or/and by its deriving hydroxyl radical as well. The basal solution used was the same as that in the aqueous Fe^{2+} and cubic pyrite oxidation experiments. Five treatments were established: (1) BI: without added H_2O_2; (2) BH: 50 $\mu mol\,L^{-1}$ H_2O_2 only; (3) BIH: 50 $\mu mol\,L^{-1}$ H_2O_2 and 55.8 $mg\,L^{-1}$ Fe^{2+}; (4) BHA: 50 $\mu mol\,L^{-1}$ H_2O_2 and 50 $\mu mol\,L^{-1}$ ascorbic acid (a scavenger of reactive oxygen species); and (5) BIHA: 50 $\mu mol\,L^{-1}$ H_2O_2, 55.8 $mg\,L^{-1}$ Fe^{2+} and 50 $\mu mol\,L^{-1}$ ascorbic acid. Only one single injection of H_2O_2 was performed for the experiment. *Acidithiobacillus ferrooxidans* were inoculated into 100 mL of a respective solution in a conical flask. The initial pH was 2 and the initial cell concentration was 3.15×10^7 cells mL^{-1}. The reactors were shaken at 130 rpm on a rotary shaker with temperature set at $30°C$. Samples were taken for cell counting after shaking for 30 min.

Analytical methods. In-situ measurement of pH and DO in the solution was made by a calibrated pH meter and DO meter, respectively. Fe^{2+} in the reacting solutions was measured by the potassium perchromate titration method[45]. Total Fe and S in the solution were determined by the inductively coupled plasma–atomic emission spectroscopy (ICP-AES). The concentration of viable planktonic cell in the reacting solutions was determined by direct cell counting using a Neubauer hemocytometer.

A FEI-XL30 environmental scanning electron microscope coupled with energy dispersive X-ray spectrometer (ESEM/EDS) was used for surface imaging and determining the surface chemical composition of the pyrite cubes. The observed surfaces were coated with a 20 nm thickness of gold. The accelerating voltage was 15 kV and the working distance was 4.9 to 6.3 mm.

XPS was employed to determine the chemical composition and element state of the mineral surfaces (to a depth of $\sim$3–5 nm). XPS analyses were performed with a Kratos Axis Ultra[DLD] spectrometer using a monochromatic Al $K\alpha$ X-rays source. Broad scan was conducted using 160 eV pass energy, while narrow high-resolution spectra of all major lines were obtained using a resolution function with a width of 0.1 eV for a pass energy setting of 40 eV. The charge effect was corrected using C 1 s from contamination at 284.6 eV. Spectra were analyzed using the CasaXPS software (Version 2.2.19). Assignment of iron and sulfur species was made by referring to the published documents (Table S1 in the Supplementary Information).

1. Alpers, C. N. & Blowes, D. W. *Environmental Geochemistry of Sulfide Oxidation. ACS Symposium Series 550.* American Chemical Society, Washington, DC. (1994).
2. Silverman, M. P. Mechanism of bacterial pyrite oxidation. *J. Bacteriol.* **94**, 1046–1051 (1967).
3. Singer, P. C. & Stumm, W. Acid mine drainage: the rate-determining step. *Science.* **167**, 1121–1123 (1970).
4. Moses, C. O., Nordstrom, D. K., Herman, J. S. & Mills, A. L. Aqueous pyrite oxidation by dissolved oxygen and by ferric iron. *Geochim. Cosmochim. Acta.* **51**, 1561–1571 (1987).
5. Olson, G. J. Rate of pyrite bioleaching by *Thiobacillus ferrooxidans*: results of an interlaboratory comparison. *Appl. Environ. Microbiol.* **57**, 642–644 (1991).
6. Evangelou, V. P. & Zhang, Y. L. A review: Pyrite oxidation mechanisms and acid mine drainage prevention. *Crit Rev Environ Sci Tech.* **25**, 141–199 (1995).
7. Bonneissel-Gissinger, P., Alnot, M., Ehrhardt, J. J. & Behra, P. Surface oxidation of pyrite as a function of pH. Environ. *Sci. Technol.* **32**, 2839–2845 (1998).
8. Edwards, K. J., Bond, P. L., Gihring, T. M. & Banfield, J. F. An archaeal iron-oxidizing extreme acidophile important in acid mine drainage. *Science.* **287**, 1796–1799 (2000).
9. Furrer, G., Phillips, B. L., Ulrich, K. U., Pothig, R. & Casey, W. H. The origin of aluminum flocs in polluted streams. *Science.* **27**, 2245–2247 (2002).
10. Rimstidt, J. D. & Vaughan, D. J. Pyrite oxidation: a state-of-the-art assessment of the reaction mechanism. *Geochim. Cosmochim. Acta.* **67**, 873–880 (2003).
11. Tyson, G. W. *et al.* Community structure and metabolism through reconstruction of microbial genomes from the environment. *Nature.* **428**, 37–43 (2004).
12. Balci, N., Shanks III, W. C., Mayer, B. & Mandernack, K. Oxygen and sulfur isotope systematics of sulfate produced by bacterial and abiotic oxidation of pyrite. *Geochim. Cosmochim. Acta.* **71**, 3796–3811 (2007).
13. Mazumdar, A., Goldberg, T. & Strauss, H. Abiotic oxidation of pyrite by Fe(III) in acidic media and its implications for sulfur isotope measurements of lattice-bound sulfate in sediments. *Chem. Geol.* **253**, 30–37 (2008).
14. Pisapia, C., Humbert, B., Chaussidon, M. & Mustin, C. Perforative corrosion of pyrite enhanced by direct attachment of *Acidithiobacillus ferrooxidans*. *Geomicrobiol. J.* **25**, 261–273 (2008).
15. Johnson, D. B. & Hallberg, K. B. Acid mine drainage remediation options: a review. *Sci. Total Environ.* **338**, 3–14 (2005).
16. Lin, C., Huang, S. & Li, Y. *Proceedings of the Joint Conference of the 6th International Acid Sulfate Soil Conference and the Acid Rock Drainage Symposium.* Guangdong Science & Technology Press, Guangzhou (2008).
17. Bae, D. Y. *et al.* Integrative ecological health assessments of an acid mine stream and in situ pilot tests for wastewater treatments. *Ecol. Eng.* **36**, 653–663 (2010).
18. Cooper, W. J., Saltzman, E. S. & Zika, R. G. The contribution of rainwater to variability in surface ocean hydrogen peroxide. *J. Geophys. Res.* **92**, 2970–2980 (1987).
19. Willey, J. D., Kieber, R. J. & Lancaster, R. D. Coastal rainwater hydrogen peroxide: Concentration and deposition. *J. Atmos. Chem.* **25**, 149–165 (1996).
20. Yuan, J. & Shiller, A. M. The variation of hydrogen peroxide in rainwater over the South and Central Atlantic Ocean. *Atmos. Environ.* **34**, 3973–3980 (2000).
21. Zuo, Y. & Deng, Y. Evidence for the production of hydrogen peroxide in rainwater by lightning during thunderstorms. *Geochim. Cosmochim. Acta.* **63**, 3451–3455 (1999).
22. Vovk, I. F. Radiolysis of underground waters as the mechanism of geochemical transformation of the energy of radioactive decay in sedimentary rocks. *Litho. Mineral. Res.* **16**, 328–334 (1982).
23. Amme, M., Bors, W., Michel, C., Stettmaier, K., Rasmussen, G. & Betti, M. Effects of Fe(II) and hydrogen peroxide interaction upon dissolving UO_2 under geologic repository conditions. *Environ. Sci. Technol.* **39**, 221–229 (2005).
24. Antonijevic, M. M., Jankovic, Z. D. & Dimitrijevic, M. D. Kinetics of chalcopyrite dissolution by hydrogen peroxide in sulphuric acid. *Hydrometallurgy.* **71**, 329–334 (2004).
25. Aydogan, S. Dissolution kinetics of sphalerite with hydrogen peroxide in sulphuric acid medium. *Chem. Eng. J.* **123**, 65–70 (2006).
26. Aydogan, S., Erdemoglu, M., Ucar, G. & Aras, A. Kinetics of galena dissolution in nitric acid solutions with hydrogen peroxide. *Hydrometallurgy.* **88**, 52–57 (2007).
27. Ehsani, M. R. Desulfurization of tabas coals using chemical reagents. *Iran. J. Chem. Chem. Eng.* **25**, 59–66 (2006).
28. Borda, M., Elsetinow, A., Schoonen, M. & Strongin, D. Pyrite-induced hydrogen peroxide formation as a driving force in the evolution of photosynthetic organisms on an early. *Earth Astrobiology.* **1**, 283–288 (2001).
29. Cohn, C. A. *et al.* Pyrite-induced hydroxyl radical formation and its effect on nucleic acids. *Geochem. Trans.* **7**, 3 (2006).
30. Schoonen, M. A. A., Harrington, A. D., Laffers, R. & Strongin, D. R. Role of hydrogen peroxide and hydroxyl radical in pyrite oxidation by molecular oxygen. *Geochim. Cosmochim. Acta.* **74**, 4971–4987 (2010).
31. Fernandez-Remolar, D. C. *et al.* The environment of early Mars and the missing carbonates. *Meteorit. Planet. Sci.* **46**, 1447–1469 (2011).
32. Haber, F. & Weiss, J. The catalytic decomposition of hydrogen peroxide by iron salts. *Proc. Roy. Soc.* **147**, 332–351 (1934).
33. Kremer, M. L. Mechanism of Fenton reaction. Evidence for a new intermediate. *PCCP.* **1**, 3595–3605 (1999).
34. Lefticariu, L., Pratt, L. M. & Ripley, E. M. Mineralogic and sulfur isotopic effects accompanying oxidation of pyrite in millimolar solutions of hydrogen peroxide at temperatures from 4 to $150°C$. *Geochim. Cosmochim. Acta.* **70**, 4889–4905 (2006).

35. Lefticariu, L., Arndt, S. A. & Pratt, L. M. Oxygen isotope partitioning during oxidation of pyrite by H_2O_2 and its dependence on temperature. *Geochim. Cosmochim. Acta.* **71**, 5072–5088 (2007).

36. Ma, Y. & Lin, C. Pyrite Oxidation under initially neutral pH conditions and in the presence of *Acidithiobacillus ferrooxidans* and micromolar hydrogen peroxide. *Biogeosciences Discuss.* **9**, 557–579 (2012).

37. Harneit, K., Göksel, A., Kock, D., Klock, J. H., Genhrke, T. & Sand, W. Adhesion to metal sulfide surfaces by cells of *Acidithiobacillus ferrooxidans*, *Acidithiobacillus thiooxidans* and *Leptospirillum ferrooxidans*. *Hydrometallurgy.* **83**, 245–254 (2006).

38. Ghauri, M. A., Okibe, N. & Johnson, D. B. Attachment of acidophilic bacteria to solid surfaces: The significance of species and strain variations. *Hydrometallurgy.* **85**, 72–80 (2007).

39. Tsuda, I., Kato, K. & Nozaki, K. Measurement of Fe^{2+} ion by coulometry method at incubation of *Thiobacillus ferrooxidans. Acta Hortic.* **440**, 75–80 (1996).

40. Buckley, A. N. & Woods, R. The surface oxidation of pyrite. *Appl. Surf. Sci.* **27**, 437–452 (1987).

41. Toniazzo, V., Mustin, C., Portal, J. M., Humbert, B., Benoit, R. & Erre, R. Elemental sulfur at the pyrite surfaces: speciation and quantification. *Appl. Surf. Sci.* **143**, 229–237 (1999).

42. Xia, J. L. *et al.* Surface analysis of sulfur speciation on pyrite bioleached by extreme thermophile Acidianus manzaensis using Raman and XANES spectroscopy. *Hydrometallurgy.* **100**, 129–135 (2010).

43. Qin, J., Li, H., Lin, C. & Chen, G. Can rainwater induce Fenton-driven degradation of herbicides in natural waters? *Chemosphere* Available online 29 March 2013, ISSN 0045-6535, 10.1016/j.chemosphere.2013.03.003.

44. Tichomirowa, M. & Junghans, M. Oxygen isotope evidence for sorption of molecular oxygen to pyrite surface sites and incorporation into sulfate in oxidation experiments. *Applied Geochemistry*, **24**(11), 2072–2092 (2009).

45. Zhou, J., Niu, Y. & Qin, W. Effects of sulfide minerals on *Acidithiobacillus ferrooxidans. Chin. J. Nonferr. Metal.* **13**, 1278–1282 (2003).

Acknowledgements

Author contributions

C.L. and Y.M. jointly designed the study. Y.M. performed the experiments and C.L. wrote the paper.

Additional information